Ionic Interactions in Crystallite Growth of CoMgAl-hydrotalcite-like Compounds

Z. P. Xu and H. C. Zeng*

Department of Chemical and Environmental Engineering, Faculty of Engineering, National University of Singapore, 10 Kent Ridge Crescent, Singapore 119260

Received March 15, 2001. Revised Manuscript Received July 16, 2001

With XRD, FTIR, CHN, ICP, and DTA/TGA techniques, ionic interactions in the forms of cation replacement/incorporation in basal layers and anion exchange/insertion in the interlayer space have been investigated. The crystallite size is increased significantly, whereas basal spacing is reduced when Co^{2+} cations or both Co^{2+} and Co^{3+} in $Co^{II}Co^{III}$-NO_3-hydrotalcite-like compound ($Co^{II}Co^{III}$-NO_3-HT) are replaced with Al^{3+} or Mg^{2+} and Al^{3+}. IR vibrational modes of hydroxyl groups and intercalated anions have been utilized in identifying exchanged interlayer species, and thermal events revealed by DTA/TGA have been correlated in verifying compositional changes and ionic interactions. In exchange experiments of Co^{II}-Co^{III}-NO_3-HT, aluminum is not only incorporated into the basal layers but is also inserted into the interlayer space (in the form of $H_2AlO_3^-$), which causes an increase in planar growth of basal layers (to about 3 times) and a similar increase (to 2−3 times) in the basal layer stacking along the *c*-axis. Other experiments for Co^{II}Al-NO_3-HT and MgAl-NO_3-HT also indicate similar increases in the planar growth (to 2−3 times) when nitrate anions are replaced by aluminate anions, although the extent of increase in layer number in the *c*-axis is not as high. It appears that stronger cation-to-anion attraction promotes the inter-basal-layer stacking in the *c*-axis, while smaller anion-to-anion lateral repulsion is beneficial to the intra-basal-layer growth; these can be practically achieved by incorporation of more trivalent cations and/or replacement of low-charged anions with higher charged ones.

Introduction

For the past decade, research in layered materials has experienced a significant growth.[1−11] In particular, intercalated compounds in which a layer of ionic or neutral chemical species is intercalated between two neighboring basal layers (i.e., in interlayer space) promise new means of tailor-making hybrid materials, e.g., inorganic−organic nanocomposites, in addition to their many known physicochemical properties and technological applications.[1,2,12] In this connection, intercalation chemistry of these layered materials is expected to gain similar attention and development as inclusion chemistry in ordered or disordered mesoporous host materials (e.g., MCM41 and other derivatives).[13−16]

Among the layered solids, hydrotalcite-like compounds (HTlcs) stand as a distinctive family and are also known as anionic clays owing to presence of negative intercalates.[1,2] In the basic structure of HTlcs, a divalent metal cation is situated in the center of oxygen octahedron formed by six hydroxyl groups. The individual octahedrons are integrated into two-dimensional infinite sheets by edge-sharing as in basal layers of brucite $Mg(OH)_2$.[1] The resultant brucite-like layers can stack upon one another to generate a three-dimensional solid via various chemical interactions between the layers. However, intercalation of organic or inorganic anions into the interlayer space occurs when divalent cations in the octahedrons are partially substituted by trivalent ones. Because extra cationic charges possessed by the trivalent cations in the brucite-like layers must be balanced by intercalated anions, an alternative stacking of bru-

* To whom correspondence should be addressed. Tel: +65 874 2896. Telefax: +65 779 1936. Email: chezhc@nus.edu.sg.

(1) Cavani, F.; Trifiro, F.; Vaccari, A. *Catal. Today* **1991**, *11*, 173.
(2) Rives, V.; Ulibarri, M. A. *Coord. Chem. Rev.* **1999**, *181*, 61.
(3) Bissessur, R.; Degroot, D. C.; Schindler, J. L.; Kannewurf, C. R.; Kanatzidis, M. G. *J. Chem. Soc. Chem. Commun.* **1993**, *8*, 687.
(4) Kerr, T. A.; Leroux, F.; Nazar, L. F. *Chem. Mater.* **1998**, *10*, 2588.
(5) Fogg, A. M.; Rohl, A. L.; Parkinson, G. M.; O'Hare, D. *Chem. Mater.* **1999**, *11*, 1194.
(6) Kumar, C. V.; Chaudhari, A. *J. Am. Chem. Soc.* **2000**, *122*, 830.
(7) (a) Eda, K. *J. Mater. Chem.* **1992**, *2*, 533. (b) Eda, K. *J. Solid State Chem.* **1989**, *83*, 292.
(8) Clearfield, A. *Chem. Mater.* **1998**, *10*, 2801.
(9) Kosuge, K.; Singh, P. S. *Chem. Mater.* **2000**, *12*, 421.
(10) Kooli, F.; Sasaki, T.; Rives, V.; Watanabe, M. *J. Mater. Chem.* **2000**, *10*, 497.
(11) (a) Zeng, H. C.; Sheu, C. W.; Hia, H. C. *Chem. Mater.* **1998**, *10*, 974. (b) Zeng, H. C.; Xu, Z. P.; Qian, M. *Chem. Mater.* **1998,** *10*, 2277. (c) Xu, Z. P.; Zeng, H. C. *Chem. Mater.* **1999**, *11*, 67. (d) Chellam, U.; Xu, Z. P.; Zeng, H. C. *Chem. Mater.* **2000**, *12*, 650. (e) Xu, Z. P.; Zeng, H. C. *Chem. Mater.* **2000**, *12*, 2597. (f) Xu, Z. P.; Zeng, H. C. *J. Phys. Chem. B* **2000**, *104*, 10 206.
(12) Butruille, J.; Pinnavaia, T. J. In *Alumina Pillared Clays in Comprehensive Supramolecular Chemistry*; Atwood, J. L., Davies, J. E. D., MacNicol, D. D., Vogtle, F., Lehn, J. M., Alberti, G., Bein, T., Eds.; Pergamon: Oxford, 1996; Vol. 7, pp 219−250.
(13) Kresge, C. T.; Leonowicz, M. E.; Roth, W. J.; Vartuli, J. C.; Beck, J. S. *Nature* **1992**, *359*, 710.
(14) Moller, K.; Bein, T. *Chem. Mater.* **1998**, *10*, 2950 and the references therein.
(15) Ying, J. Y.; Mehnert, C. P.; Wong, M. S. *Angew. Chem., Int. Ed.* **1999,** *38*, 56 and the references therein.
(16) Thomas, J. M. *Angew. Chem., Int. Ed.* **1999**, *38*, 3588 and the references therein.

10.1021/cm010222b CCC: $20.00
Published on Web 10/12/2001

Table 1. Synthetic Conditions for the Precursor Hydrotalcite-like Compounds and Their Derived Compounds

sample	method	temp, °C	aging time, h	atmosphere (mL·min^{-1})	pH[c]	preparation procedures
A1	PA[a]	37	24	O_2 (40)	8.0	20 mL of 1.0 M Co^{2+} nitrate solution + 100 mL of 0.5 M $NH_3{\cdot}H_2O$
A2	AE[b]	25	4	N_2 (60)	13−14	$^1/_3$ A1 slurry + 100 mL of 0.2 M $NaAl(OH)_4$ + 0.8 M NaOH
A3	PA	25	24	O_2 (40)	13−14	20 mL of 1.0 M $Co(NO_3)_2$ + 100 mL of 0.5 M $NH_3{\cdot}H_2O$ + 0.2 M $NaAl(OH)4$[d] + 0.8 M NaOH
B1	PA	60	24	N_2 (60)	8.0	20 mL of Co^{2+} + Al^{3+} nitrate solutione + 100 mL of 0.5 M $NH_3{\cdot}H_2O$
B2	AE	25	4	N_2 (60)	13−14	$^1/_3$ B1 slurry + 100 mL of 0.2 M $NaAl(OH)_4$ + 0.8 M NaOH
B3	AE	25	4	N_2 (60)	12.0	$^1/_3$ B1 slurry + 100 mL of 0.2 M Na_2CO_3
C1	PA	60	24	static air	9.5	20 mL Mg^{2+} + Al^{3+} nitrate solutione + 100 mL of 1.0 M $NH_3{\cdot}H_2O$
C2	AE	25	4	static air	13−14	$^1/_3$ C1 slurry + 100 mL of 0.2 M $NaAl(OH)_4$ + 0.8 M NaOH
C3	AE	25	4	static air	8.0	$^1/_3$ C1 slurry + 100 mL of 0.2 M NH_4HCO_3

[a] PA represents precipitation then aging method. [b] AE represents anion-exchange method. [c] pH value in final filtrate solution. [d] The number indicates the equivalent aluminate anion is 0.2 M. [e] Total cation concentration is 1.0 M with the divalent to trivalent cation ratio = 2:1.

cite-like layer and intercalate layer results in the same structure as natural hydrotalcite, $Mg_6Al_2(OH)_{16}CO_3{\cdot}4H_2O$.[1]

It has been known that large molecular or polymeric anions (up to a few tens of angstroms) can be intercalated between the basal layers with certain prediction for guest orientations.[5,17,18] Using metal oligomeric species (oxometalates), mesoporous oxometalate-pillared HTlcs can be prepared.[2,19] One distinguished physicochemical property of HTlcs is their chemical exchangeability with other chemical species. Apart from chemical exchange for the interlayer anions,[1,2] metal cations in the brucite-like layers can also participate in exchange with other cationic species in solution.[20] Furthermore, if more trivalent cations are incorporated into the brucite-like layers, a new run of anion intercalation will commence accordingly. All these physicochemical processes are governed by both thermodynamics and reaction kinetics and will lead to formation of more stable final compounds.

Along the course of the above chemical exchanges, physical processes also proceed simultaneously. For instance, enlarging or reducing interlayer space and changing crystallographic dimensions of crystallites take place inevitably due to new types of ionic interactions in the exchanged compounds. To the best of our knowledge, among these fundamental processes, crystallite growth during the ionic exchanges has not been examined systematically so far, although it has been observed in many HTlcs during aging treatment.[21,22] In this work, effects of both cationic and anionic exchanges/insertions and thus of new ionic interactions on the crystallite growth of HTlcs will be investigated with XRD, FTIR, EA (CHN and ICP), and DTA/TGA with respect to the preparation methods.

Experimental Section

Sample Preparation. Samples A1, A3, B1, and C1 listed in Table 1 were prepared by a precipitation−aging method. Briefly, 20 mL of nitrate salt solution (total cation concentration is 1.0 M; $Co(NO_3)_2{\cdot}6H_2O$ from Fluka, >99.0%; $Mg(NO_3)_2{\cdot}6H_2O$ from Merck, 99%; $Al(NO_3)_3{\cdot}9H_2O$ from Merck, 98.5%) were added dropwise to 100 mL of 0.5 M $NH_3{\cdot}H_2O$ (A1 and B1) or 1.0 M $NH_3{\cdot}H_2O$ (C1) or to 100 mL of 0.5 M $NH_3{\cdot}H_2O$ + 0.2 M $NaAl(OH)_4$ + 0.8 M NaOH solution (A3) in 10 min under stirring. After aging for 24 h at 25 °C (A3), 37 °C (A1), or 60 °C (B1 and C1) respectively in oxygen, nitrogen, or air environment, the precipitates were collected by filtration and fully washed with deionized water, followed by drying at room temperature in vacuo overnight. The optimal experimental conditions adopted above (such as aging temperature) were to achieve high crystallinity and purity for the final products.

Other samples (A2, B2, B3, C2, and C3, Table 1) were obtained by anion exchange method. In general, one-third of the above precipitates (slurry, ca. 400−600 mg of dry precipitate) was transferred to a three-necked round-bottom flask, which was precharged with an aluminate anion solution (100 mL of 0.2 M equiv of $Al(OH)_4^-$ and 0.8 M NaOH) or with a carbonate anion solution (100 mL of 0.2 M CO_3^{2-} or HCO_3^-). The exchange reactions were continued for 4 h under protection of nitrogen (A2, B2, and B3) or in static air (C2 and C3). The posttreatments were the same as above and the relevant parameters were detailed in Table 1.

The mixture solution of 0.2 M $NaAl(OH)_4$ and 0.8 M NaOH was prepared by partially dissolving 4.0 g of $Al(OH)_3$ in 120 mL of 1.0 M NaOH with gentle heating at 80 °C for 2−3 h under the protection of nitrogen. After standing overnight, the transparent liquid consisted of 0.2 M equiv of $NaAl(OH)_4$, as measured with inductively coupled plasma (ICP) atomic emission spectroscopy for Al^{3+} concentration. It should be mentioned that this solution also contained a small amount of CO_3^{2-} anions owing to strong absorption of ambient CO_2 in NaOH solution.

Materials Characterization. Crystallographic information on the samples was investigated by powder X-ray diffraction (XRD). Diffraction patterns of intensity versus 2θ were recorded with a Shimadzu XRD-6000 X-ray diffractometer with Cu Kα radiation (λ = 1.5418 Å) from 8 to 70° at a scanning speed of 1 deg·min^{-1}. The interlayer spacing of the resultant HTlcs and other layered cobalt hydroxides was determined from the diffraction peak positions/patterns with structural analysis software and the average size of precipitate crystallites was estimated by the Debye−Scherrer's formula.[23] Chemical bonding information on metal−oxygen, hydroxyl, and intercalated functional groups (such as nitrate and carbonate anions) was investigated with Fourier transform infrared spectroscopy (FTIR, Bio-Rad, model FTS 3500) using the potassium bromide (KBr) pellet technique. Each FTIR spectrum was collected after 40 scans with a resolution of 2 cm^{-1}.

Nitrogen and carbon contents of the as-prepared samples were measured in a Perkin-Elmer 2400 CHN analyzer, while the aluminum, magnesium, and cobalt contents were determined by inductively coupled plasma (ICP) atomic emission

(17) Ding, W. P.; Gu, G.; Zhong, W.; Zang, W. C.; Du, Y. W. *Chem. Phys. Lett.* **1996**, *262*, 259.
(18) Oriakhi, C. O.; Farr, I. V.; Lerner, M. M. *J. Mater. Chem.* **1996**, *6*, 103.
(19) Trifiro, F.; Vaccari, A. In *Solid State Supramolecular Chemistry: Two- and Three-Dimensional Inorganic Networks in Comprehensive Supramolecular Chemistry*; Atwood, J. L., Davies, J. E. D., MacNicol, D. D., Vogtle, F., Lehn, J. M., Alberti G., Bein, T., Eds.; pp 251−291, Pergamon: Oxford, 1996; Vol. 8, pp 251−291.
(20) (a) Komarneni, S.; Kozai, N.; Roy, R. *J. Mater. Chem.* **1998**, *8*, 1329. (b) Fujii, S.; Sugie, Y.; Kobune, M.; Touno A.; Touji, J. *Nippon Kagaku Kaishi* **1992**, 1504.
(21) Ookubo, A.; Ooi, K.; Hayashi, H. *Langmuir* **1993**, *9*, 1418.
(22) Miyata, S. *Clays Clay Miner.* **1980**, *28*, 50.
(23) Cullity, B. D. *Elements of X-ray Diffraction*, 2nd ed.; Addison-Wesley: MA, 1978.

Table 2. Crystallite Size (*D*) and Distances (*d*) between Reflection Planes from XRD Data

	crystallite size, nm			dist btwn reflectn planes, Å							
sample	D_{003}	D_{110}	D_{003}/D_{110}	d_{003}[b]	d_{006}[b]	d_{009},[b] d_{012}	d_{015}	d_{018}	d_{110}[b]	d_{113}	$d_{1,0,16}$
A1	7(9)[a]	8	0.87	7.98	3.97	2.61	2.31		1.540		
A2	15(20)	27	0.55	7.524	3.763	2.580	2.287	1.934	1.532	1.501	1.42
A3	25(33)	27	0.92	7.516	3.759	2.65, 2.59	2.29	1.94	1.532	1.501	1.42
B1	13(13)	13	1.00	8.903	4.447	2.64			1.530	1.51	1.45
B2	15(20)	28	0.53	7.563	3.781	2.65, 2.59	2.29		1.534	1.503	1.42
B3	14(18)	19	0.74	7.556	3.767	2.65, 2.59	2.30		1.532	1.501	1.42
C1	13(15)	12	1.08	8.901	4.451	2.57	2.38	2.10	1.520	1.503	
C2	13(16)	21	0.62	7.598	3.801	2.57, 2.52	2.31	1.94	1.522	1.493	1.41
C3	14(20)	21	0.67	7.588	3.789	2.58, 2.52	2.31	1.97	1.521	1.492	1.41

[a] The number in parentheses is the average brucite-like-layer number. [b] Lattice parameter $c = 3d_{003} \approx 6d_{006} \approx 9d_{009}$ (c is vertical length of unit cell in 3R symmetry, rombohedral) and $a = 2d_{110}$ (a is lattice parameter of the hexagonal subcell that contains two OH groups).

spectroscopy (Perkin-Elmer ICP OTIMA 3000). The trivalent cobalt content was determined by a redox reaction. Typically, 20.00 mg of solid sample was dissolved in 40.0 mL of 1.0 M HCl solution with gentle heating. The produced Cl_2 gas (from Cl^-) was gradually purged with N_2 at 40 mL·min^{-1} and sent to a flask containing 50.0 mL of 0.01 M KI solution mixed with starch indicator. The resultant blue mixture was then titrated against a $Na_2S_2O_3$ solution (0.0050 M) until the blue coloration disappeared.

Studies with differential thermal analysis (DTA, Shimadzu DTA-50) and thermogravimetric analysis (TGA, Shimadzu TGA-50) were carried out to understand thermal behaviors of the as-prepared samples. In the DTA study, the heating was conducted in air atmosphere (air flow rate = 40 mL·min^{-1}) from 40 to 700 °C at a rate of 10 °C·min^{-1}. To further explain the DTA results, TGA measurement was carried out from 40 to 700 °C under the same conditions as those used in DTA.

Results and Discussion

Characterization of Layered Structures. XRD patterns of all nine samples are shown in Figure 1. For sample A1, the diffraction peak shapes and positions (2θ angles) are the same as those of our previous work,[24,25] which is indicative of a typical hydrotalcite-like structure. The basal spacing for A1 is 7.98 Å, as listed in Table 2, noting that (110) and (113) peaks are overlapped at $2\theta = 60-62°$.

Compared to A1, sample A2 (synthesized by dipping A1 in aluminate solution, Table 1) was much better crystallized. For example, all diffraction peaks become much narrower, as shown in Figure 1, and particularly, the peaks of (110) and (113) are distinctly separated at $2\theta = 60-62°$. Some weak diffractions, such as those of planes (009), (012), (015), (018), and (1010), which are not shown in A1, can be clearly observed now.[1,2] In addition, peak positions of (00l) are shifted to higher angles and the basal spacing is somewhat compressed (d_{003} = 7.524 Å, Table 2) due to the replacement of weakly bonded NO_3^- by aluminate anions. The d_{003} distance of A2 is close to those of $Co^{II}Al$-HT-CO_3 (7.33 Å)[26] and of sample A3 (7.516 Å, Table 2) that was also prepared in $Al(OH)_4^-$ solution (Table 1). However, sample A3 does not exhibit the strong diffraction peaks of (015), (018), and (1010), which indicates some difference in crystallite orientation, size, and/or texture between A2 and A3, noting the preparation methods for them are different, although their basic crystallographic structures are identical.

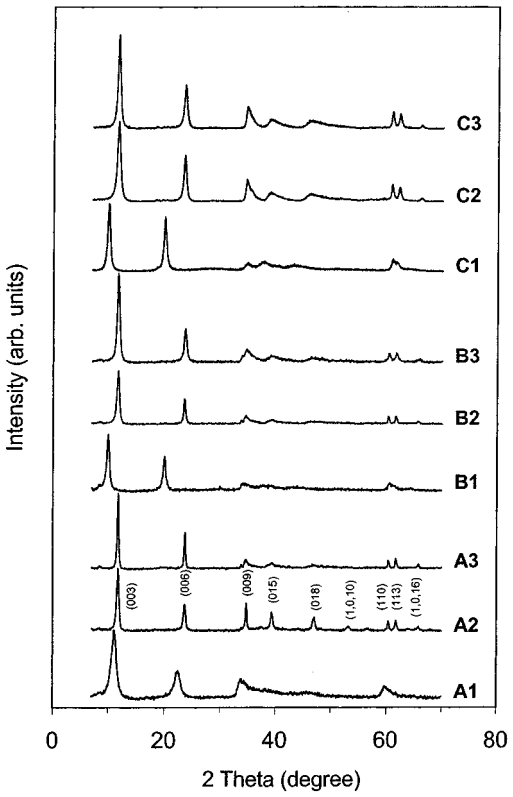

Figure 1. XRD patterns measured for the samples of A1−A3, B1−B3, and C1−C3.

When Co^{2+} cations or both Co^{2+} and Co^{3+} in samples A1−A3 ($Co^{II}Co^{III}$-HT) are replaced by Al^{3+} or Mg^{2+} and Al^{3+} similar XRD peak shift and enhancement have also been observed for samples B1−B3 ($Co^{II}Al$-HT) and C1−C3 (MgAl-HT) in Figure 1. Apart from the two strong peaks (003) and (006), there is only an overlapped band at around 61° (consisting of (110) and (113) diffractions) for B1 and C1, while there are two distinct peaks (110) and (113) for the remaining four samples. It is again noted that the basal distance (d_{003}, Table 2) is decreased to a similar extent after samples B1 and C1 were immersed respectively in aluminate or carbonate solution, which indicates that the intercalated NO_3^- anions were exchanged with aluminate and/or carbonate anions. In the latter two series (B2−B3 and C2−C3), nevertheless, the diffraction peaks corresponding to planes of (009), (012), (015), and (018) are weak and broad, unlike in sample A2.

FTIR peaks/bands and their respective assignments of the as-prepared samples are listed in Table 3 for

(24) Xu, Z. P.; Zeng, H. C. *J. Mater. Chem.* **1998**, *8*, 2499.
(25) Xu, Z. P.; Zeng, H. C. *Chem. Mater.* **2000,** *12*, 3459.
(26) Kannan, S.; Swamy, C. S. *J. Mater. Sci. Lett.* **1992**, *11*, 1585.

Table 3. Some Typical Vibrational Modes and Their Wavenumbers in FTIR Spectra

sample[a]	A1	A2	A3	B1	B2	B3	C1	C2	C3
ν(OH)	3500 (b,st)	3460 (b,st)	3450 (b,st)	3540 (b,m)	3440 (b,st)	3450 (b,st)	3570 (b,st)	3480 (b,m)	3470 (b,m)
		3090 (sd,w)	3090 (sd,w)	3450 (b,m)	3100 (sd,w)	3100 (sd,w)	3480 (b,st)	3100 (sd,w)	3100 (sd,w)
$\delta(H_2O)$	1640 (b,m)	1650 (b,m)	1650 (b,m)	1650 (b,w)	1650 (b,m)	1650 (b,m)	1660 (b,w)	1650 (b,w)	1650 (b,w)
δ(OH)	640 (b,st)	791 (b,st)	798 (b,st)	710 (b,m)	798 (b,st)	800 (b,st)	673 (b,st)	786 (b,st)	788 (b,st)
$\nu_3(NO_3^-)$	1384 (sh,st)		1384 (sd,vw)	1384 (sh,st)		1384 (sd,w)	1384 (sh,st)		
$\nu_3(CO_3^{2-})$		1358 (sh,st)	1356 (sh,st)		1362 (sh,st)	1355 (sh,st)		1359 (sh,st)	1359 (sh,st)
$\nu_2(NO_3^-)$	839 (sh,vw)			827 (sh,w)			827 (sh,w)		
	827 (sh,w)								
$\nu_2(CO_3^{2-})$		860 (sd,w)	860 (sd,w)		860 (sd,w)	860 (sd,w)		860 (sd,w)	860 (sd,w)
$\nu_4(CO_3^{2-})$		680 (sd,w)	680 (sd,w)		680 (sd,w)	680 (sd,w)			
lattice	860 (b,m)	597 (sh,m)	612 (sh,m)	607 (sh,m)	610 (sh,m)	610 (sh,m)	840 (b,m)	945 (b,w)	948 (b,w)
(M−O)	561 (sh,m)	549 (sh,m),	549 (sh,m)	550 (sd,w)	547 (sh,m)	547 (sh,m)	550 (sh,m)	678 (sh,m)	680 (sh,m)
	518 (sh,m)	422 (sh,st)	424 (sh,st)	421 (sh,st)	424 (sh,st)	424 (sh,st)	446 (sh,m)	552 (sh,m)	552 (sh,m)
								448 (sh,st)	449 (sh,st)

[a] b stands for broad, sh for sharp, sd for shoulder, st for strong, m for medium, w for weak, and vw for very weak.

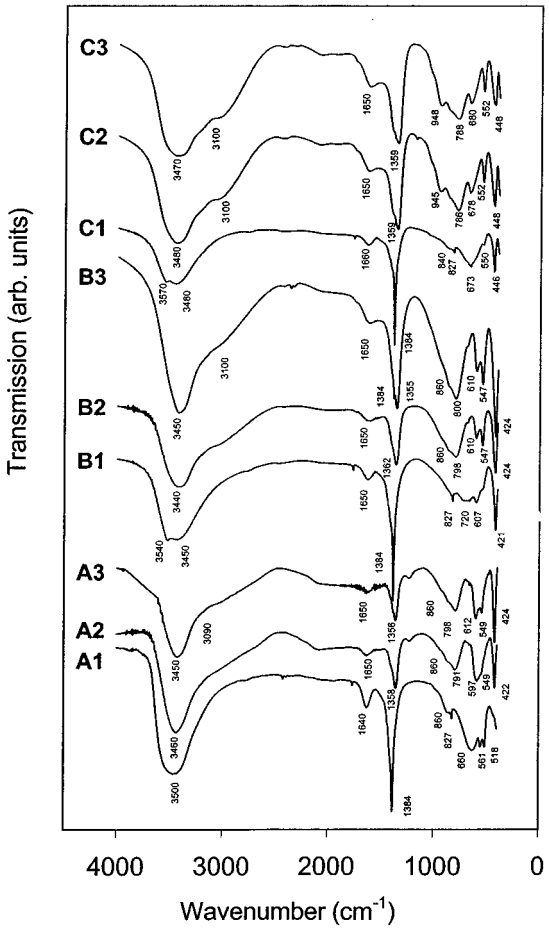

Figure 2. FTIR spectra of the samples of A1−A3, B1−B3, and C1−C3.

comparison. The FTIR spectra in Figure 2 indicate that the interlayer NO_3^- anions in the initial samples of A1, B1, and C1 are in a relatively unperturbed state. This is evidenced by the strong IR absorption peak at 1384 cm^{-1} that is assigned to symmetrical stretching vibration mode of NO_3^- (ν_3 mode; with D_{3h} symmetry).[11b,11c,25,27] Moreover, this NO_3^- peak disappears after samples A1, B1, and C1 were immersed respectively in aluminate or carbonate solution. New IR absorption peaks at 1355−1362 cm^{-1} are attributed to the ν_3 mode of CO_3^{2-} and the wavenumber observed is also indicative of a nearly unperturbed state for CO_3^{2-} in the interlayer.[1,27,28]

It is worthwhile mentioning that the band shapes and positions of ν_{OH} and δ_{OH} are changed accordingly when there is an anion exchange. As observed, the ν_{OH} band at 3500 cm^{-1} of A1 is broader than those of A2 and A3.[27−29] A shoulder appears at higher wavenumber for B1 (3540 cm-[1]) and C1 (3570 cm-[1]), which indicates clearly that there are two main types of hydroxyl groups in the brucite-like layers.[30] Since a large interlayer space 4.1 Å (= 8.9−4.8 Å) is found for the B1 and C1 compounds, it is our belief that the interlayer NO_3^- anions may tend to stick to only one side (instead of two sides), noting that the thickness of a flat-lying NO_3^- is only 2.8 Å.[31] This proposed anion configuration has been supported in our recent study for NO_3-containing MgAl−HTlcs, which suggests that the hydroxyls in the brucite-like layers can be divided into two groups in accordance with the two IR absorptions (at 3540−3570 cm^{-1} and 3450−3480 cm^{-1}) in samples B1 and C1.[30] A broad shoulder at 3090−3100 cm^{-1} (ν_{OH}) can be observed for samples A2, A3, B2, B3, C2, and C3.[27−29] At the same time, the δ_{OH} vibration frequency shifts up from 660−720 cm^{-1} (A1, B1, and C1) to 786−800 cm^{-1} (A2, A3, B2, B3, C2, and C3)[27] when the interlayer NO_3^- was replaced with other anions. These two IR observations suggest a stronger hydrogen bonding interaction between the water molecules and the newly intercalated anions (CO_3^{2-} and/or $H_2AlO_3^-$), which will be discussed shortly.

Crystallite Growths. Crystallite dimensions in the crystallographic directions of [003] (or [00*l*], Table 2) and [110] (denoted as D_{003} and D_{110}, respectively) are calculated with Scherrer's equation using the full width at half-maximum intensity (fwhm) of corresponding diffraction peaks.[23] To get the precise fwhm's for A1, B1, and C1, overlapping bands at 60−62° were deconvoluted into (110) and (113) peaks without peak width constraint, as shown in Figure 3. The results in Table

(27) (a) Delahaye-Vidal, A.; Ehlsissen, K. T.; Genin P.; Figlarz, M. *Eur. J. Solid State Inorg. Chem.* **1994**, *31*, 823. (b) Elsissen, K. T.; Delahaye-Vidal, A.; Genin, P.; Figlarz, M.; Willmann, P. *J. Mater. Chem.* **1993**, *3*, 883.

(28) Hernandez-Moreno, M. J.; Ulibarri, M. A.; Rendon J. L.; Serna, C. J. *Phys. Chem. Miner.* **1985**, *2*, 34.

(29) Fernandez, J. M.; Barriga, C.; Ulibarri, M. A.; Labajos F. M.; Rives, V. *J. Mater. Chem.* **1994**, *4*, 1117.

(30) Xu, Z. P.; Zeng, H. C. *J. Phys. Chem. B* **2001**, *105*, 1743.

(31) Pauling, L. *The Nature of the Chemical Bond*; Cornell University Press: New York, 1948; pp 187−191.

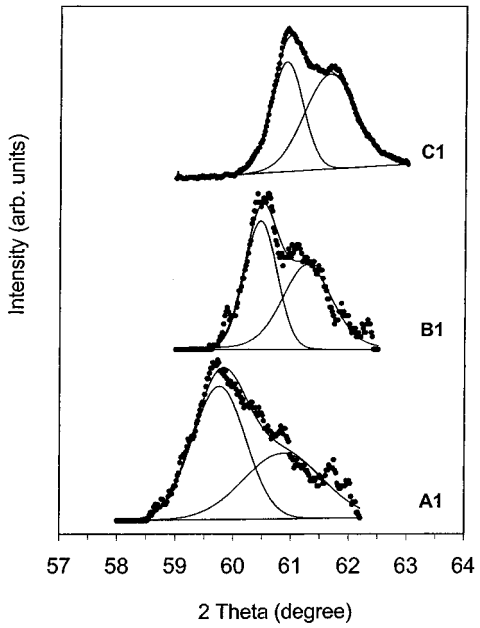

Figure 3. Deconvolution of (110) and (113) peaks (Figure 1) for samples A1, B1, and C1.

2 indicate that the D_{110} data are increased to about 2−3 times after the precursor samples (A1, B1, and C1) were immersed in an aluminate or carbonate solution. This increase indicates that crystallites further grow along the [110] direction of the hydrotalcite-like structure (3*R* symmetry, rhombohedral)[1,21,22] or that there is an intraplanar growth of basal layers in general. The D_{003} data of A2 and A3 are also increased to about 2−3 times, compared to that of A1. Although the apparent dimension in the [003] direction in B2, B3, C2 and C3 is about the same as that of B1 and C1, the number of brucite-like layers is actually increased by about 10−50% (indicated by the number in parentheses of Table 2), since the d_{003} is compressed by ∼15% after the anion exchange (note the disappearance of the IR peak of nitrate at 1384 cm^{-1} in Figure 2).

The observed dimensional increases of the hydrotalcite-like crystallites are clearly associated with the change of the intercalated anions. For example, it is well-known that there is stronger electrostatic interaction between carbonate anions and the brucite-like sheets, owning to the double charge of the anions (compared to the monocharge anion NO_3^-).[1,22] Apparently, the high charge of the anion as well as its chemical nature may be related to the observed crystallite growths. To exclude other possible causes such as high pH values in the experiments of A2 and A3, sample A1 was also placed in a 1.0 M NaOH solution for 16 h with air bubbling. Interestingly, it all converted into cobaltic acid ($HCoO_2$), which is shown in Figure 4.[32] Furthermore, FTIR spectra in Figure 5 also give unique vibration bands of this compound at 580 and 1221 cm^{-1}.[33] Even under the protection of nitrogen, the sample in 1.0 M NaOH (A1) still changed into a mixture of brucite-like cobalt hydroxide β-$Co(OH)_2$ and cobaltic acid $HCoO_2$. As can be noted in Figures 4 and 5, the presence of β-$Co(OH)_2$ is confirmed by the sharp diffraction peaks in Figure 4 and the IR absorptions at 3629 and 505 cm^{-1}.[11c] The above two experiments ruled out the possible cause of high pH exchange medium to the crystallite growths, which will be further discussed below.

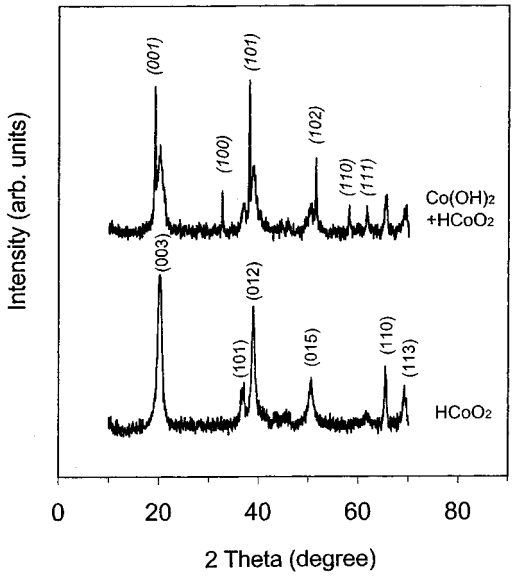

Figure 4. XRD patterns of A1 treated in 1.0 M NaOH solution in air bubbling for 16 h ($HCoO_2$) or in N_2 bubbling for 4 h ($Co(OH)_2$ + $HCoO_2$) at 25 °C.

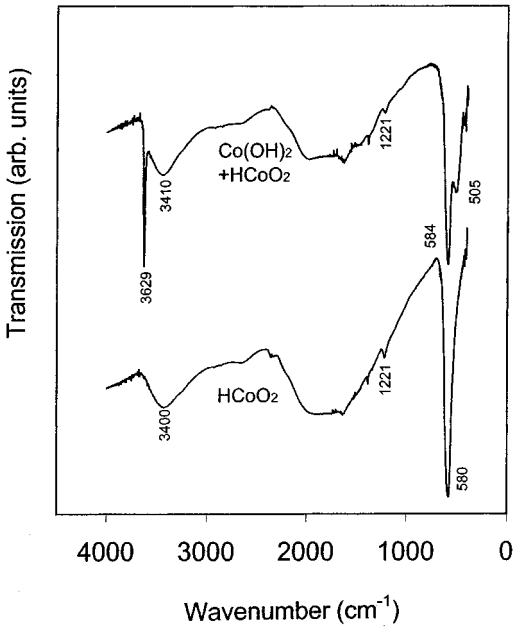

Figure 5. FTIR spectra of A1 treated in 1.0 M NaOH solution in air bubbling for 16 h ($HCoO_2$) or in N_2 bubbling for 4 h ($Co(OH)_2$ + $HCoO_2$) at 25 °C.

Determination of Chemical Formulas. The results of elemental measurements (see Experimental Section) and related structural/compositional analyses are summarized in Table 4. As can be noted, a trace amount of CO_3^{2-} is intercalated into the interlayer space for all the precursor compounds (A1, B1, and C1). The content of CO_3^{2-} is increased significantly in all aluminate anion containing samples (A2, A3, B2, and C2), while it becomes the only interlayer anions in the

(32) Powder Diffraction Files for $HCoO_2$, Card Nos. 07-0169, 14-0673, and 26-1107, Joint Committee on Powder Diffraction Standards, Swarthmore, PA, 1995.

(33) Delaplane, R. G.; Ibers, J. A.; Ferraro J. R.; Russ, J. J. *J. Chem. Phys.* **1969**, *50*, 1920.

Table 4. Results of Elemental Analysis

sample	%Co[a]	%Mg[a]	%Al[a]	%C[a]	%N[a]	M^{III}/M[b]	A^-/M[b]	$A_{Al}{}^-/M$[b]	TA/M'[c]	$M^{III\prime}/M'$[c]	chemical formula[d]
A1	45.9			0.21	2.20	0.25	0.25		0.25	0.25	$Co^{II}_{0.58}Co^{III}_{0.19}(OH)_{1.54}(CO_3)_{0.02}(NO_3)_{0.15}\cdot 0.9H_2O$
A2	36.8		6.73	1.04	0.0	0.51	0.20	0.155	0.39	0.38	$Co^{II}_{0.47}Co^{III}_{0.16}Al_{0.13}(OH)_{1.51}(CO_3)_{0.09}(H_2AlO_3)_{0.12}\cdot 1.1H_2O$
A3	34.7		8.17	0.81	0.18	0.44	0.17	0.135	0.35	0.35	$Co^{II}_{0.50}Co^{III}_{0.09}Al_{0.18}(OH)_{1.55}(CO_3)_{0.07}(H_2AlO_3)_{0.12}\cdot 1.1H_2O$
B1	31.9		7.22	0.09	3.91	0.33	0.36		0.36	0.33	$Co^{II}_{0.54}Al_{0.27}(OH)_{1.59}(CO_3)_{0.01}(NO_3)_{0.28}\cdot 0.9H_2O$
B2	35.5		8.39	0.72	0.01	0.34	0.13	0.105	0.27	0.27	$Co^{II}_{0.60}Al_{0.22}(OH)_{1.64}(CO_3)_{0.06}(H_2AlO_3)_{0.10}\cdot 1.1H_2O$
B3	34.6		8.02	1.89	0.10	0.34	0.36		0.36	0.34	$Co^{II}_{0.59}Al_{0.30}(OH)_{1.76}(CO_3)_{0.16}\cdot 1.0H_2O$
C1		16.7	9.33	0.17	4.76	0.34	0.36		0.36	0.34	$Mg_{0.69}Al_{0.35}(OH)_{2.07}(CO_3)_{0.01}(NO_3)_{0.34}\cdot 1.0H_2O$
C2		19.2	11.02	1.29	0.03	0.34	0.18	0.08	0.29	0.28	$Mg_{0.79}Al_{0.31}(OH)_{2.19}(CO_3)_{0.11}(H_2AlO_3)_{0.10}\cdot 1.2H_2O$
C3		17.8	10.32	2.45	0.00	0.34	0.37		0.37	0.34	$Mg_{0.73}Al_{0.38}(OH)_{2.20}(CO_3)_{0.20}\cdot 1.2H_2O$

[a] Weight percentage; the ratio $[Co^{III}]/([Co^{II}]+[Co^{III}])$ is 0.25, 0.25, and 0.15 for A1, A2, and A3, respectively. [b] $M = T_{Al} + [Mg] + [Co]$; $M^{III} = T_{Al} + [Co^{III}]$; $A^- = 2[CO_3^{2-}] + [NO_3^-]$; and $A_{Al}{}^- = [H_2AlO_3^-]$. [c] $TA = 2[CO_3^{2-}] + [NO_3^-] + A_{Al}{}^-$; $M' = T_{Al} + [Mg] + [Co] - A_{Al}{}^-$; and $M^{III\prime} = [Co^{III}] + T_{Al} - A_{Al}{}^-$. [d] Chemical formula $Co^{II}aMg_bCo^{III}cAl_d(OH)_e(CO_3)_f(NO_3)_g(H_2AlO_3\text{-})_h\cdot nH_2O$ is calculated on the basis of 100 g of sample; n includes about $0.5H_2O$ in inter-crystallite pores (i.e., non interlayer water) based on the TGA results (Table 5).

aluminate anion free samples (B3 and C3, Table 4). For samples A1, B1, B3, C1, and C3, the obtained M^{III}/M (the molar ratio of all trivalent to total metal cations) and A^-/M (the molar ratio of negative charges carried by CO_3^{2-} and NO_3^- to total metal cations) are very close to each other, which indicates a good electric neutralization between positively charged brucite-like layers and the negative interlayer anions. However, for samples A2, A3, C2, and B2, M^{III}/M is much greater than that of the corresponding $2CO_3^{2-}/M$ (NO_3^- can be ignored in these samples, Table 4). Furthermore, the large M^{III}/M values (0.51 and 0.44) for samples A2 and A3 are out of the range for a pure hydrotalcite-like phase (the value is normally 0.2−0.4).[1,2] The inconsistency between M^{III}/M and $2CO_3^{2-}/M$ indicates that part of aluminum cations exist in the form of aluminate anions in the interlayer space. The amount of alunimate anion A_{Al}- can be estimated through the charge and mass balances:

$$[Co^{3+}] + [Al^{3+}] = A_{Al}{}^- + 2[CO_3{}^{2-}] \quad (1)$$

$$T_{Al} = [Al^{3+}] + A_{Al}{}^- \quad (2)$$

where $[Al^{3+}]$ is the amount of aluminum cations in the brucite-like layers and T_{Al} is the total amount of aluminum atoms. Thus, by adding (1) with (2), we have

$$A_{Al}{}^- = {}^1/_2\{T_{Al} + [Co^{3+}] - [CO_3{}^{2-}]\} \quad (3)$$

The calculation results, as listed in Table 4, indicate that there is 30−50% of aluminum in the form of aluminate anions intercalated in the interlayer space of samples A2, A3, B2, and C2.

To find out a specific species of aluminate anions in the interlayer space, we had considered some simple aluminate anions, such as $Al(OH)_4^-$, $H_2AlO_3^-$, and AlO_2^-.[34,35] In terms of the system energy, $Al(OH)_4^-$ is more favorable and usually the predominant form in the basic solution, as reported in the literature.[34,35] Subtracting the basal spacing (d_{003}, Table 2) with the thickness of a brucite-like layer (4.8 Å) gives the *c*-dimension occupied by the aluminate and/or carbonate anions of 2.7−2.8 Å. The dimension of tetrahedral geometry of $Al(OH)_4^-$ anion is 5.2 Å along its C_3 axis or 4.7 Å along its C_2 axis, noting that the van der Waals' radius of oxygen is 1.4 Å.[31] Obviously, the size of this tetrahedral aluminate anion is simply too big for the observed interlayer space. However, the thickness of a planar $H_2AlO_3^-$ or the width of a linear AlO_2^- is 2.8 Å (van der Waals' diameter of oxygen).[31] These two forms of aluminates are suited closely to our observed interlayer spaces (2.7−2.8 Å):

$$Al(OH)_4{}^- \rightarrow H_2AlO_3{}^- + H_2O \quad (4)$$

$$Al(OH)_4{}^- \rightarrow AlO_2{}^- + 2H_2O \quad (5)$$

According to eq 4, the intercalation of $H_2AlO_3^-$ occurs in high pH solution. It has been reported in the literature that containing this aluminate anion in the interlayer space of MgAl-HTlcs causes no noticeable change of the basal spacing.[36] Compared to $H_2AlO_3^-$, formation of AlO_2^- in deep dehydration reaction is much less plausible because eq 5 is thermodynamically unfavorable.[37] On the basis of elemental analysis and the above aluminate anion assignment (to $H_2AlO_3^-$), the chemical formulas for the as-prepared hydrotalcite-like compounds (Table 1) can now be deduced and they are summarized in Table 4.

Ionic Interactions upon Thermal Decomposition. To understand ionic interactions in the as-prepared HTlcs, results from thermal investigation shown in Figures 6 and 7 will be further discussed. The DTA curve of A1 is the same as that in our early report,[25] showing the dehydration occurring at 148 °C and collapse of layered structure at 174 °C. The two thermal events are also reflected in their corresponding differential TGA (DrTGA) curves (Figure 7). When the nitrate anions are replaced, the dehydration of surface-adsorbed water (i.e., in intercrystallite pores) in samples A2 and A3 can be observed at ca. 80 °C in Figure 6. Furthermore, the broad endothermic bands at 137 and 141 °C (Figure 6) and at 150 and 157 °C (Figure 7, DrTGA), corresponding to two medium weight losses at 11.0% (ended at 186 and 194 °C, respectively, Table 5), can be assigned to the removal of intercalated water molecules which form hydrogen bonds with aluminate

(34) Chen, N.; Liu, M.; Cao, Y.; Tang, B.; Hong, M. *Sci. China (Ser. B)* **1993**, *36*, 32.
(35) Barcza, L.; Palfavi-Rozsahegyi, M. *Mater. Chem. Phys.* **1989**, *21*, 345.
(36) Lukashin, A. V.; Kalinin, S. V.; Nikiforov, M. P.; Privalov, V. I.; Eleseev, A. A.; Vertegel A. A.; Tretyakov, Y. D. *Dokl. Akad. Nauk.* **1999**, *364*, 77.
(37) Specific reaction enthalpy change and free-energy change for $Al(OH)_4^-(aq) = AlO_2^-(aq) + 2H_2O(l)$ are $\Delta H_r^o = 0$ kJ·mol^{-1} and $\Delta G_r^o = 0.2$ kJ·mol^{-1}, respectively, using thermodynamic data from: (a) *CRC Handbook of Chemistry and Physics*, 80th ed., Lide, D. R., Ed.; CRC Press: 1999; pp 5−86. (b) Wu, C. H.; Dobrogowska, C.; Zhang, X.; Hepler, L. G. *Can. J. Chem.* **1997**, *75*, 1110.

Table 5. Results of Thermogravimetric Analysis

sample	WL1	WL2	WL3	WL4
A1	12.6% at 182 °C	28.1% at 400 °C	28.3% at 500 °C	
A2	11.0% at 186 °C	25.5% at 400 °C	26.6% at 500 °C	
A3	11.0% at 194 °C	25.9% at 400 °C	27.2% at 500 °C	
B1	6.8% at 196 °C	34.6% at 400 °C	35.3% at 500 °C	
B2	12.2% at 196 °C	27.9% at 400 °C	28.9% at 500 °C	
B3	16.5% at 260 °C	28.7% at 400 °C	30.1% at 500 °C	
C1	9.9% at 220 °C	11.0% at 300 °C	48.2% at 600 °C	48.6% at 700 °C
C2	11.1% at 220 °C	19.6% at 300 °C	41.4% at 600 °C	42.2% at 700 °C
C3	16.6% at 300 °C	42.5% at 600 °C	43.3% at 700 °C	

[a] WL indicates the total weight loss of sample at a given temperature.

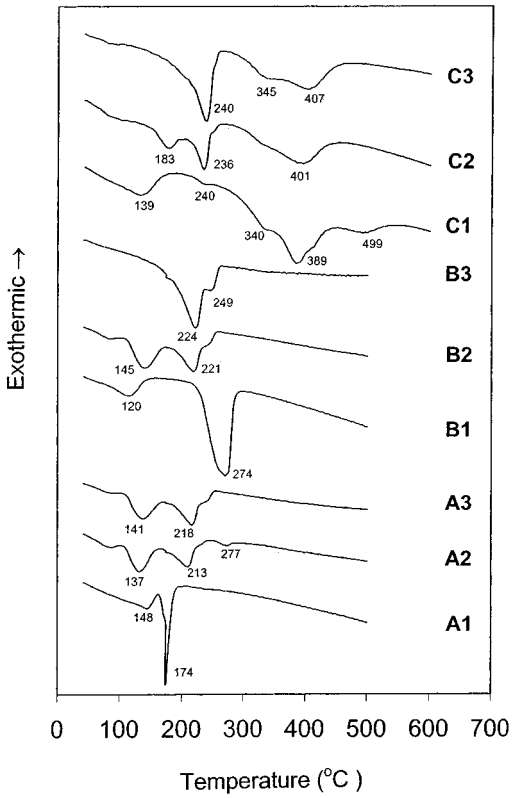

Figure 6. DTA scanning curves of the samples of A1−A3, B1−B3, and C1−C3 in air (air flow rate = 40 mL·min^{-1}).

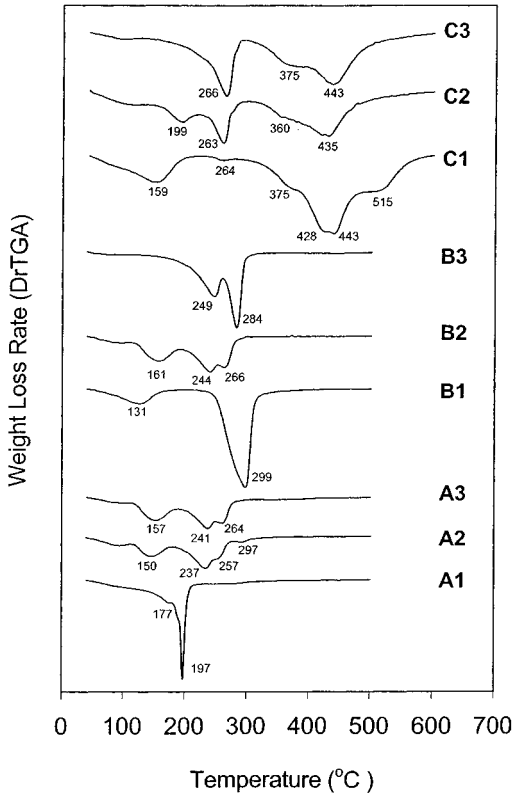

Figure 7. DrTGA curves deduced from TGA scanning for the samples of A1−A3, B1−B3, and C1−C3 in air (air flow-rate = 40 mL·min^{-1}).

anions ($H_2O\cdots H_2AlO_3^-$) in the interlayer space. The depletion of CO_3^{2-} and the breakdown of hydrotalcite-like structure take place at higher temperatures, i.e., at 213 and 218 °C, respectively, noting that a small dip at 277 °C in A2 is due to the thermal decomposition of an intermediate compound $HCoO_2$ during the heating process.[39]

Sample B1 undergoes two distinct thermal events (Figures 6 and 7). The broad band around 120 °C corresponds to the dehydration of various water molecules, and the stronger endothermic peak at 274 °C is attributed to the total thermal effect of the dehydroxylation of brucite-like layers, depletion of NO_3^-, and oxidation of divalent cobalt.[40] As expected, thermal decomposition behavior of sample B2 (Figure 6) is quite similar to those of A2 and A3, since they have similar structure and composition. Sample B3 shows two overlapped thermal events (224 and 249 °C, Figure 6) that are clearly separated in its DrTGA curve at around 249 and 284 °C (Figure 7). Based on the TGA data (Table 5), the removal of interlayer water and the depletion of carbonate anions should occur in the first endothermic stage,[25] while the collapse of the layered structure (endothermic) and a partial oxidation of divalent cobalt (exothermic) occur the second stage, where the two different thermal effects may partially cancel each other in the DTA signal (i.e., the small peak at 249 °C).

In sample C1, the interlayer water is readily removed at 139 °C and all hydroxyl groups are removed in the range 340−389 °C (Figure 6). The decomposition of trace CO_3^{2-} is also noted at about 240 °C (as a small dip).[1,28,41−43] As for NO_3^-, it may attach to a metal cation (M) during the dehydroxylation at 340−389 °C, forming

(38) Akitt, J. W.; Gessner W.; Weinberger, M. *Magn. Reson. Chem*., **1988**, *26*, 1047.
(39) (a) Avramov, L. K. *Thermochim. Acta* **1973**, *10*, 409. (b) Brien, P. O.; Patel, U. *J. Chem. Soc., Dalton Trans.* **1982**, 1407.
(40) del Arco, M.; Trujillano R.; Rives, V. *J. Mater. Chem*. **1998**, *8*, 761.
(41) Tsuji, M.; Mao, G.; Yoshida, T.; Tamaura, Y. *J. Mater. Res.* **1993**, *8*, 1137.
(42) Yun, S. K.; Pinnavaia, T. J. *Chem. Mater*. **1995**, *7*, 348.
(43) Marino, O.; Mascolo, G. *Proc. 2nd Eur. Symp. Thermal Anal.* **1981**, 391.

an intermediate species M···O−NO_2.[11d] A broad endothermic band at around 499 °C (Figures 6) is thus attributable to the decomposition of M···O−NO_2. Unlike C1, sample C2 shows a small peak at 183 °C that may be assigned to the dehydration of hydrogen-bonded water with the aluminate anions in the interlayer (H_2O···$H_2AlO_3^-$), similar to the cases of A2, A3, and B2. As reported in the literature,[43] OH intercalated hydrotalcite-like compound $Mg_{0.7}Al_{0.3}(OH)_2(OH)_{0.3}\cdot nH_2O$ exhibits an endothermic band at 215 °C (DTA), which has been assigned to the removal of interlayer water molecules (H_2O···OH). Apparently, this temperature (215 °C) is much higher than what we observed in C2. The water removed at 183 °C is thus associated to aluminate anions. The peak at 236 °C is caused by the depletions of CO_3^{2-} and its related water. The peaks at 340 and 401 °C (Figure 6) can be assigned respectively to the dehydroxylations of Al-connecting and Mg-connecting OH groups. As a typical hydrotalcite compound, sample C3 exhibits the same decomposition process as those reported in the literature.[1,28,43] Except for the lack of the 183 °C peak, the remaining peak assignments are similar to those of C2 (Figure 6), noting that C3 contains no $H_2AlO_3^-$. The DrTGA results in Figure 7 reflect essentially the same information as those in Figure 6.

Ionic Interactions and Crystallite Growths. It has been reported that the divalent cations in the brucite-like layers of hydrotalcite-like compounds can be exchanged with the other divalent cations in the aqueous solution. This exchange might be due to the higher aqueous equilibrium concentration of divalent cations.[20] As a rough approximation, one can estimate the magnitude of cation concentration from the solubility product of individual hydroxides.[44] For example, in a solution with pH = 10−13 (Table 1), cation concentrations of the current systems can be calculated as $[Mg^{2+}] + [Mg(OH)^+] = 10^{-6}-10^{-3}$ M, $[Co^{2+}] + [Co(OH)^+] = 10^{-11}-10^{-8}$ M, $[Al^{3+}] + [Al(OH)^{2+}] + [Al(OH)_2^+] = 10^{-14}-10^{-11}$ M, and $[Co^{3+}] + [Co(OH)^{2+}] + [Co(OH)_2^+] = 10^{-20}-10^{-15}$ M. Higher solution concentrations of divalent cations mean more dissolution and thus more reprecipitation that will lead to more divalent cation exchange. Compared to those of divalent cations, the equilibrium concentrations of trivalent cations in solution phase are much lower in the pH range under study.

In our current syntheses for samples A2, A3, B2, and C2, nonetheless, the concentrations of trivalent cations (aluminate anions) in the initial solutions are not low (Table 1), which will lead to incorporation of trivalent cations into the brucite-like layers. Indeed, the incorporation of trivalent cations (Al^{3+}) is evidenced in A2 (transformed from A1). After the experiment, the trivalent to total metal ratio ($M^{III\prime}/M'$, Table 4) has been changed from 0.25 (A1) to 0.38 (A2), while $[Co^{III}]/([Co^{II}] + [Co^{III}])$ remains unchanged. This observation indicates that there is a considerable degree of material incorporation that includes both Al^{3+} cations in the brucite-like sheets and $H_2AlO_3^-$ anions in the interlayer space, noting that the charges are well-balanced. The easy incorporation is further evidenced in A3 synthesis (Table 1), in which the population of trivalent cobalt in the compound is significantly reduced as the trivalent cations can directly come from the solution Al^{3+} rather than depending on the oxidative generation of trivalent cobalt.[11b,c] The introduction of Al^{3+} and $H_2AlO_3^-$ into originally aluminum-free sample A1 would cause restructuring (dissolution and reprecipitation/recrystallization) original crystallites of A1, resulting in highly crystalline sample A2.

One phenomenon observed along with the crystallite growth is the intercalation of double-charged anions CO_3^{2-} in the interlayer space. For the monocharged anion NO_3^--containing samples A1, B1, and C1 (they are almost CO_3^{2-}-free), the D_{110} values are generally small. This can be explained by the spatial crowdedness of the anions in the interlayer space. To maintain the commensurate electric-charge balance, there must be a critical dimension (D_{110}) of crystallites which limits the growth within the basal planes. This can be described as a commensurate-to-incommensurate transition due to a large number of the intercalated monocharged anions. In replacing NO_3^-, the number of CO_3^{2-} can be reduced by 50% and the incommensurate charge array appears no longer a hindrance for the growth. From sample A1 to samples A2 and A3 (Table 4), for example, the molar ratio of double-charged anions to total anions in the interlayer space increases from 0.12 to 0.43 and 0.37, respectively, and similar observations can also be obtained for sample series B1−B3 (0.03, 0.38, and 1.00) and C1−C3 (0.03, 0.52, and 1.00). These data indicate a decrease in crowdedness for the anions and thus lower anion−anion repulsion within the interlayer space.

In addition to the above comparisons on the absolute dimensions of crystallites, relative dimension data (D_{003}/D_{110}, Table 2) allow us to have a better view on various ionic interactions during the crystallite growths. For NO_3^- anion containing samples A1, B1, and C1, the D_{003}/D_{110} data are 0.87, 1.00, and 1.08, respectively. The slight increase in the latter two samples is attributed to stronger ionic interactions between M^{III} (more Al^{3+} cations, Table 4) and NO_3^-, which promotes the growth along [00*l*] direction. For samples A2 and A3, which have great variation in M^{III} species but similar interlayer anions, the significant increase in D_{003}/D_{110} data indicates that Al^{3+} has stronger ionic interaction than Co^{3+} with the intercalated anions. Similar trends in D_{003}/D_{110} data can be observed for samples B2 and B3, as well as for samples C2 and C3 (Tables 2 and 4). In all the cases, stronger cation-to-anion attraction promotes the inter-brucite-like-layer stacking while smaller anion-to-anion lateral repulsion is beneficial to the intra-brucite-like-layer growth.

Conclusions

In summary, the crystallite size of HTlcs can be increased significantly when Co^{2+} cations or both Co^{2+} and Co^{3+} in $Co^{II}Co^{III}$-NO_3-HT (A1) are replaced with Al^{3+} (B1) or Mg^{2+} and Al^{3+} (C1); the exchange/replacement is also accompanied by a reduction in basal spacing. IR vibrational modes of hydroxyl groups and intercalated anions can be utilized in finding exchanged species in the interlayer space. Furthermore, the resultant compositional changes and related ionic interactions can be verified with DTA/TGA methods by examining patterns of interlayer water releasing and collapse

(44) Smith, R. M.; Martell, A. E. *Critical Stability Constants*; Plenum Press: New York, 1989; Vol. 4, Inorganic Complexes, p 6.

temperature of the layered compounds. It is found that the aluminum is not only incorporated into the brucite-like layers of $Co^{II}Co^{III}$-NO_3-HT as cations but also inserted into the interlayer space as anions ($H_2AlO_3^-$) in replacing nitrate ions, which causes an increase in planar growth of basal layers to about 3 times and a similar increase (to 2−3 times) in the basal layer stacking in the *c*-axis. Increases in planar growth (to 2−3 times) are also observed in $Co^{II}Al$-NO_3-HT (B1) and MgAl-NO_3-HT (C1) when nitrate anions are replaced, although the increase in *c*-axis stacking is reduced to a smaller extent of 10−50%. In all cases, stronger cation-to-anion attraction promotes the inter-brucite-like layer stacking in *c*-axis while smaller anion-to-anion lateral repulsion is beneficial to the intra-brucite-like layer growth. The growths can be actually achieved by incorporating more trivalent cations into the brucite-like layers and/or reducing crowdedness of anions in the interlayer space with replacement of higher charged anions.

Acknowledgment. We gratefully acknowledge research funding (RP3999902/A and A/C50384) co-supported by the Ministry of Education and the National Science and Technology Board of Singapore. Z.P.X. thanks the Chemical and Process Engineering Center, National University of Singapore, for providing financial support for postgraduate study.

CM010222B